1-5-2020

Near-Field Pressure Signature Splicing for Low-Fidelity Design Space Exploration of Supersonic Aircraft

Christian R. Bolander
Utah State University, christian.bolander@aggiemail.usu.edu

Douglas F. Hunsaker
Utah State University, doug.hunsaker@usu.edu

Recommended Citation

Bolander, Christian R., and Douglas F. Hunsaker. "Near-field Pressure Signature Splicing for Low-Fidelity Design Space Exploration of Supersonic Aircraft." AIAA Scitech 2020 Forum. 2020.

Near-field Pressure Signature Splicing for Low-Fidelity Design Space Exploration of Supersonic Aircraft

Christian R. Bolander* and Douglas F. Hunsaker†
Utah State University, Logan, UT, 84321

As interest in supersonic overland flight intensifies, new ways to meet government restrictions on sonic boom loudness must be implemented. Low-fidelity aerodynamic tools, such as PANAIR, can estimate the near-field pressure signature that ultimately determines the loudness of the sonic boom at the ground. These tools can greatly benefit the exploration of large design spaces due to their computational efficiency. One of the limitations of low-fidelity tools is the accuracy of the solution produced, which is dependent on the fundamental physical assumptions made in the development of the governing equations. If flow patterns are produced that severely violate these fundamental assumptions, the validity of the near-field pressure signature is compromised. A method is proposed that splices together near-field pressure signatures from a low-fidelity and a higher-fidelity tool by cutting each pressure signature at a critical point and then blending the low-fidelity signature into the higher-fidelity signature. By splicing the signatures together, sections of the low-fidelity signature that represent fundamental violations of the governing equation are removed. This method allows for the exploration of the design space corresponding to areas on the geometry that produce accurate results in a low-fidelity signature. The method is tested on the JAXA Wing Body geometry from the Second AIAA Sonic Boom Prediction Workshop and shows that perturbations to this geometry can produce loudness results that match the higher-fidelity results to within 0.4 PLdB.

I. Nomenclature

L	=	aircraft reference length
M_∞	=	freestream Mach number
p	=	local pressure
p_o	=	overpressure
p_∞	=	freestream pressure
P	=	near-field pressure predicted by PANAIR
S_{xx}	=	signal power per frequency
t	=	time
U	=	near-field pressure predicted by UNS3D
x	=	axial location
x_b	=	non-dimensional axial location to begin signature blending
x_c	=	non-dimensional axial cutting location
x_0	=	initial axial location in near-field pressure signature
ϵ_b	=	relative blending error
ϕ_{xx}	=	second derivative of the velocity potential with respect to x
ϕ_{yy}	=	second derivative of the velocity potential with respect to y
ϕ_{zz}	=	second derivative of the velocity potential with respect to z
ω	=	blending function

*Ph.D. Student, Mechanical and Aerospace Engineering, 4130 Old Main Hill, AIAA Student Member.
†Assistant Professor, Mechanical and Aerospace Engineering, 4130 Old Main Hill, AIAA Member.

II. Introduction

Recent efforts to optimize aircraft for drag and loudness have yielded point-designs, which produce the optimal drag and loudness for a specific flight condition [1–3]. When flown at a different flight condition, the aircraft can experience significant increases in loudness or drag depending on the changes in flight and atmospheric conditions. The NASA University Leadership Initiative (ULI) program titled "Adaptive Aerostructures for Revolutionary Civil Supersonic Transportation" (hereafter referred to as "the ULI program") has focused its efforts on expanding the optimal flight envelope of supersonic aircraft through changing the outer mold line (OML) of the aircraft using shape-memory alloys (SMAs). By making small changes or deformations to an aircraft geometry, it has been found that sonic boom loudness can be decreased for off-design flight conditions [4, 5].

Predicting sonic boom loudness follows the procedure outlined in Fig. 1. First, a description of the OML of the aircraft geometry is defined, which is then used in an aerodynamic model to measure pressure perturbations at some radial distance from the center-line of the body. The pressure perturbations are represented in the form of a near-field pressure signature. In three-dimensions, the pressure perturbations create a near-field pressure cone around the aircraft that can be sampled at various azimuthal angles to obtain the slice shown in Fig. 1.

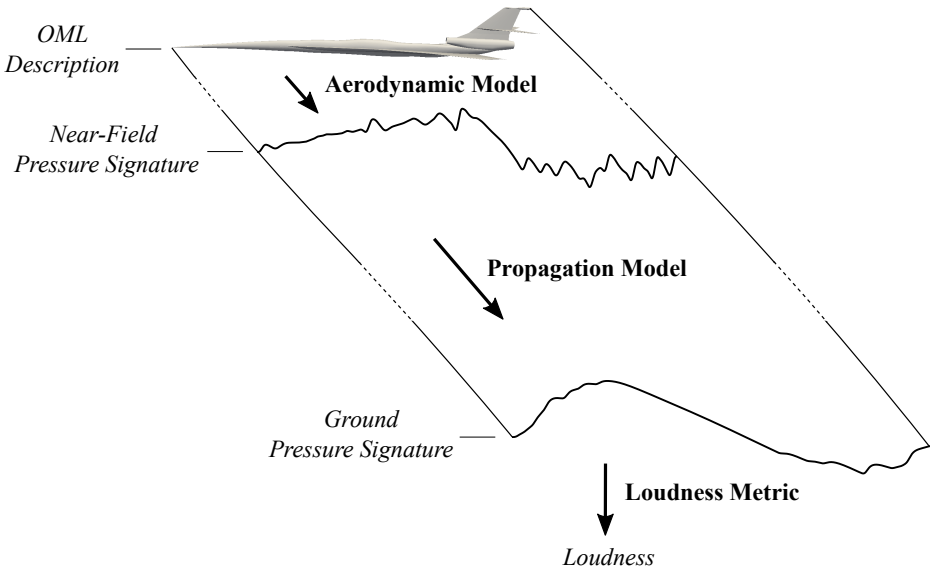

Fig. 1 A representation of the procedure used for the prediction of sonic boom loudness.

The near-field pressure signature at a given azimuthal angle is propagated through the atmosphere to the ground, where it is referred to as a ground pressure signature. Throughout the history of sonic boom loudness prediction, several metrics have been used to quantify the effective loudness that bystanders perceive on the ground. It has been found that the perceived level metric can predict the loudness of sonic booms perceived by the human ear more accurately than other methods [6–9].

The process outlined in Fig. 1 shows that changes to the OML of the aircraft directly affect the near-field pressure signature, which changes the loudness perceived when the signature reaches the ground. An example of a near-field signature is shown in Fig. 2, where the vertical axis represents the local deviation from the freestream pressure, called the overpressure, and the horizontal axis shows the distance of the sampled signature from the location of initial measurement normalized by the reference length of the body. The location at which the near-field pressure signature is sampled is generally reported as a certain number of body lengths away from the center-line of the body, i.e. $R/L = 3$. Pressure disturbances in supersonic flow propagate along and downstream of the Mach cone of the aircraft, a slice of which is shown in Fig. 1. As such, the aircraft creates pressure disturbances that propagate farther downstream than the length of the body, resulting in values on the x-axis that are greater than 1.

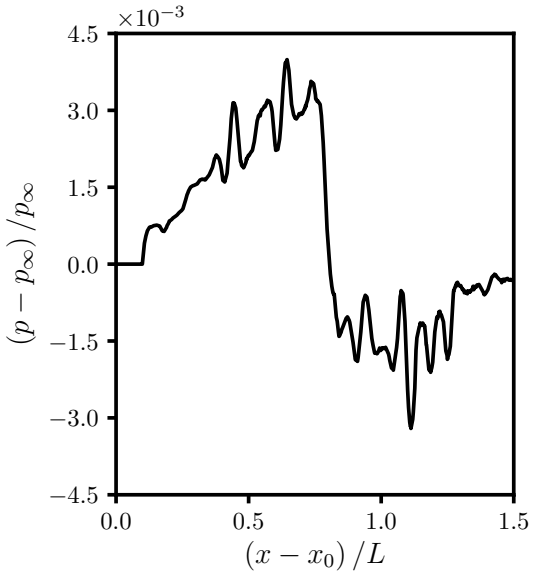

Fig. 2 An example near-field pressure signature.

The perceived level metric calculates the loudness by analyzing the energy contained in various frequency ranges in the ground pressure signature [10, 11]. As such, the power spectrum of a ground signature, which gives a representation of the energy per unit frequency contained in each frequency component of a signal, can give insight into the loudness predicted by the perceived level metric. The power spectrum found after propagating the signature in Fig. 2 to the ground can be seen in Fig. 3.

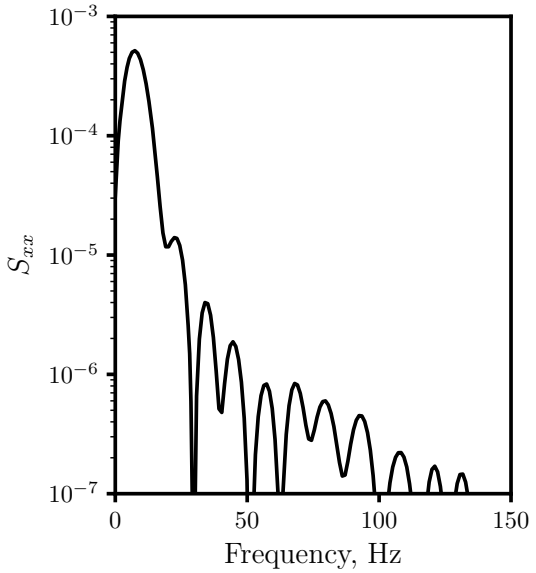

Fig. 3 The power spectrum of a sample ground pressure signature.

The design space created when looking at changes to the entirety of the OML of the aircraft is very large and well-suited for a multi-fidelity optimization framework [12]. In the multi-fidelity optimization framework proposed by the ULI program, low-fidelity aerodynamic solvers are used to explore the general design space, while high-fidelity aerodynamic solvers execute targeted studies in locations of interest. The objective is to find key trade-offs between loudness and drag for various flight conditions. The need for the low-fidelity tools cannot be understated, as the time savings are crucial to providing a thorough exploration of the general design space. Even as computational power

increases, there is a need for accurate, low-fidelity tools that can be used to inform design choices.

Since the efficiency of this multi-fidelity optimization framework is dependent on the performance of low-fidelity tools, it is crucial to understand the limitations inherent in the implementation of these tools. The low-fidelity aerodynamic tool used in this work is PANAIR (A502), a three-dimensional panel method, which was developed by Boeing and NASA [13–18]. PANAIR can be used to find flow-field properties for both subsonic and supersonic flows [19].

PANAIR solves for supersonic flow conditions using the Prandtl-Glauert equation for linearized compressible flow

$$\left(1 - M_\infty^2\right) \phi_{xx} + \phi_{yy} + \phi_{zz} = 0 \tag{1}$$

As a linearized equation, the application of the Prandtl-Glauert equation requires that the magnitude of deviations from the freestream velocity, called perturbation velocities, are much less than the magnitude of the freestream velocity. Large changes in perturbation velocity occur in areas of the aircraft geometry with high curvature, which correspond to the presence of stronger shock waves. Equation (1) also requires that the flow never produces transonic or hypersonic flow regions. A severe violation of any of these assumptions will greatly reduce the accuracy of the flow-field solution produced by PANAIR [20].

When compared to a higher-fidelity solver, such as an Euler solution, the PANAIR results are in good agreement for a wide range of geometries [4, 12, 20–22]. The axisymmetric body used by Giblette and Hunsaker [4], for example, is long, slender, and has very gradual changes in geometry, which result in low perturbation velocities and no strong shocks in the flow. All of these factors lead to a solution from PANAIR that matches very well with higher-fidelity aerodynamic solvers, with a loudness difference on the order of 0.1-0.6 PLdB [20].

In contrast, Giblette [20] and others [5] have demonstrated that a wing-body geometry produced poor results in PANAIR when compared to an Euler solution due to violations of the assumptions made by the Prandtl-Glauert equation. Large perturbation velocities and a localized transonic region caused the last 20% of the near-field pressure signature to exhibit large pressure spikes that result in a vast over-prediction of the sonic boom loudness. While the first 80% of the near-field signature matched very well with the Euler solution, changes to the geometry in this region did not produce the same change in loudness that was calculated in the Euler solution. This indicates that simply calibrating the results given by PANAIR by some fixed loudness will not bridge the gap between the results given by PANAIR and those produced by an Euler solution. These issues limit the use of this geometry in a multi-fidelity optimization framework.

The intent of the present work is to introduce a method for splicing together a near-field signature from a low-fidelity tool, such as PANAIR, with a near-field signature from a high-fidelity tool. This will allow PANAIR to be used as part of a multi-fidelity framework with geometries that produce poor off-body results in certain regions, such as the geometry used by Giblette [20] and Carpenter et al. [5]. Assuming that the deformations made to the geometry are small and do not significantly alter the lift generated by the body, the change in the near-field signature should not have a significant effect downstream of the deformation. A design space consisting of geometric variability of the aircraft geometry with constant flight conditions can then be explored on the section of the aircraft that is in good agreement with the Euler solution without regard to sections of the geometry producing poor results.

III. Tool and Geometry Descriptions

This section will describe the tools that are used in the sonic boom loudness prediction procedure outlined in Fig. 1. In addition, the baseline geometry and the deformation applied to it will be introduced. These geometries will be used to test the near-field signature splicing method and help define its limits.. The tools used in this framework have been used in previous work presented by the NASA ULI program and have been shown to provide accurate predictions of sonic boom loudness [4, 5, 11, 23]. The baseline geometry presented here is taken from the Second AIAA Sonic Boom Prediction Workshop, which also furnished CFD meshes for each geometry [24].

Figure 4 shows the tools used at each step of the procedure outlined in Fig. 1. Since different aerodynamic solvers require different geometry descriptions, the aerodynamic solvers were chosen first and the necessary OML descriptions were chosen to meet solver needs. The low-fidelity tool used in this study is PANAIR, the three-dimensional panel method mentioned previously. The high-fidelity tool is UNS3D, a Navier-Stokes flow solver developed by Texas A&M University that can solve for both inviscid and viscous flows [25]. In this work, UNS3D will be used exclusively as an inviscid Euler solver and anytime the name of the solver is used, it will be referring to an Euler solution. The UNS3D cases shown here were evaluated in a previous work by Carpenter et al. [5] and additional information about the solution setup can be found in that work.

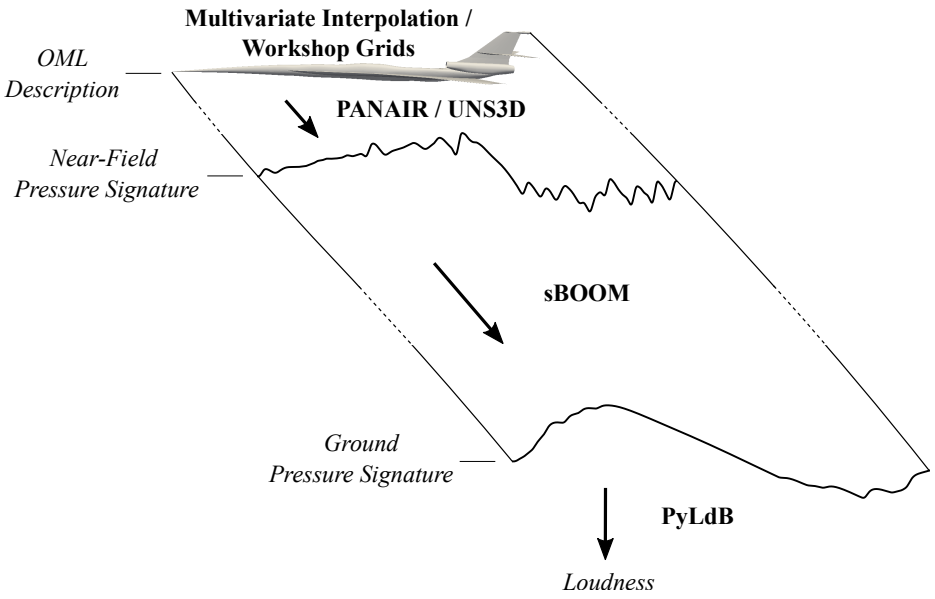

Fig. 4 An overview of the tools used in the prediction of sonic boom loudness.

As a panel method, PANAIR requires a structured surface mesh of the geometry to produce results. In contrast to PANAIR, UNS3D uses an unstructured volume mesh to solve for flow properties that is identical to those provided by the Second AIAA Sonic Boom Prediction Workshop for the inviscid case [24]. Due to hard-coded limits on the number of panels in PANAIR, multivariate interpolation was performed on the UNS3D surface grid to construct a surface mesh for PANAIR with an appropriate panel density. Constructing the grid using interpolation allowed for a representation of the geometry that very closely approximated the representation used in UNS3D, minimizing the geometrical error between the meshes.

The near-field signature generated by the aerodynamic solvers is propagated to the ground using sBOOM, a tool developed by NASA that solves the augmented Burgers' equation and includes the effects of molecular relaxation and thermovisous absorption [26–29].The loudness is calculated using an implementation of Stevens' Mark VII algorithm in PyLdB*, an open-source tool developed by Utah State University [11]. This tool has been found to provide accurate results for the calculation of sonic boom loudness and has been benchmarked against NASA's Loudness Code for Asymmetric Sonic Booms (LCASB), which is a well-accepted code for perceived level loudness calculation [5, 11].

The geometry used in this work is the JAXA Wing Body (JWB) geometry [30], shown in Fig. 5. The JWB was created to produce the same under-track equivalent area distribution as the NASA Configuration 25D (NASA 25D) low-boom concept aircraft [2, 3]. The flight conditions for the JWB are identical to those specified in the Second AIAA Sonic Boom Prediction Workshop [24]. Of particular note is that the reference length, L, for the JWB is not the body length (38.7 m), but rather equal to the body length of the NASA 25D (32.92 m) as used by Park and Nemec [24] and Ueno et al. [30].

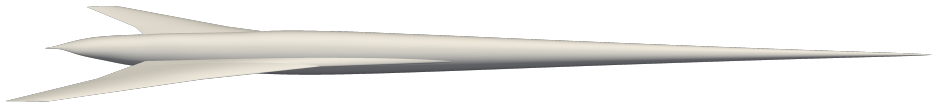

Fig. 5 A rendering of the JAXA Wing Body (JWB) geometry.

To study the effectiveness of the near-field splicing method on a perturbed geometry, the baseline JWB geometry was deformed into what will be referred to in this work as the JWB-bump geometry. The JWB-bump geometry is the

*https://github.com/usuaero/PyLdB

same deformed geometry used by Carpenter et al. [5], with a Gaussian-shaped perturbation centered at 7.74 meters from the nose and a maximum deformation of 3 cm. Figure 6 shows a rendering of the JWB-bump geometry (blue) with the baseline JWB geometry (black) for comparison.

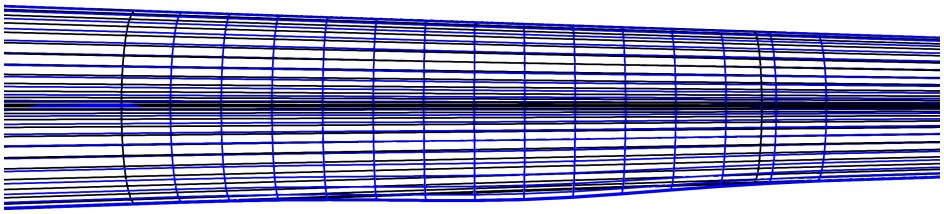

Fig. 6 Rendering of the deformation on the JWB-bump geometry and its comparison to the baseline geometry.

Figure 7 shows the nomenclature for the sections of the JWB and JWB-bump geometries that will be used when referring to the respective meshes. The deformed mesh for the JWB-bump geometry is shown in Fig. 8 and Table 1 shows the number of panels corresponding to each section of both geometries. As PANAIR is able to impose a plane of symmetry on the flow, only one half of the geometry is needed as an input to PANAIR, which is reflected in the number of panels in Table 1.

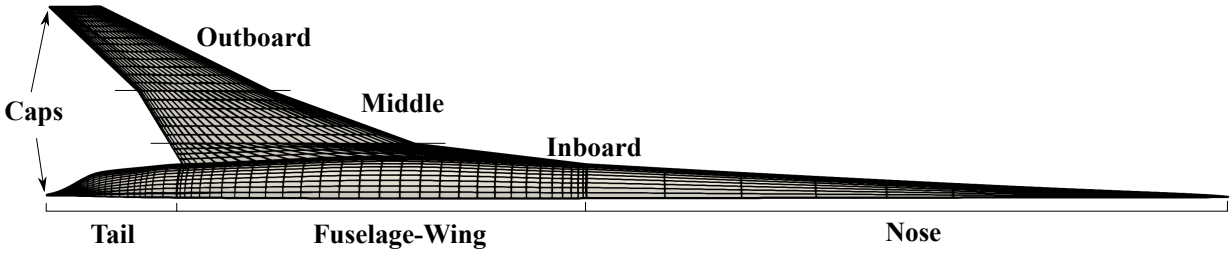

Fig. 7 Mesh and section nomenclature for the baseline JWB geometry.

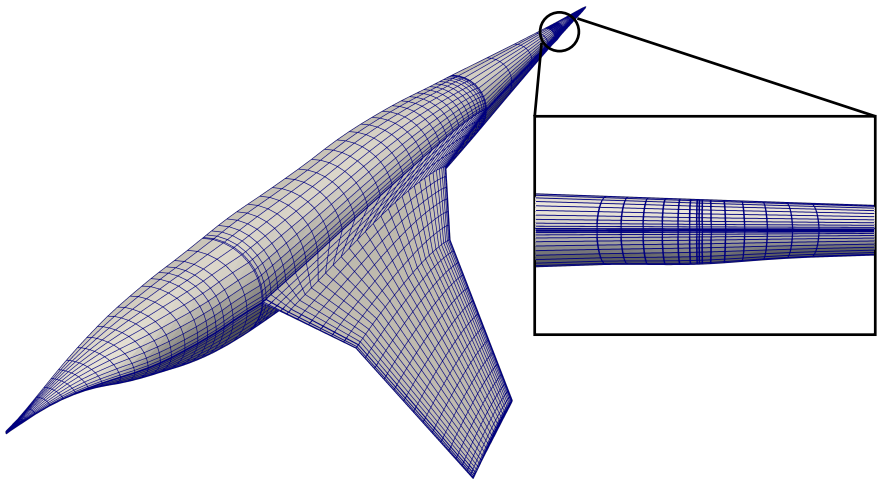

Fig. 8 Mesh for the JWB-bump geometry.

Table 1 Number of PANAIR surface mesh panels for the baseline JWB and JWB-bump geometries.

Wing

Panel Orientation	Inboard	Middle	Outboard	Cap
Span-wise	4	6	16	1
Chord-wise	32	32	32	32
Total Panels		1824*		

Fuselage (JWB)

Panel Orientation	Nose	Fuselage-Wing	Tail	Cap
Axial	13	32	20	1
Circumferential	30	30	30	30
Total Panels		1980*		

Fuselage (JWB-bump)

Panel Orientation	Nose	Fuselage-Wing	Tail	Cap
Axial	23	32	20	1
Circumferential	26	26	26	26
Total Panels		1950*		

*Note that the entire geometry has twice the listed number of panels.

A grid convergence study was previously performed on the baseline JWB geometry [20] and was extended to the JWB-bump deformation. Panels were cosine-spaced in the axial direction about the center of the deformation to improve resolution in the center of the deformation where the curvature was more pronounced. Three levels of grid resolution were tested: a coarse mesh with 6 panels, a medium mesh with 10 panels, and a fine mesh with 14 panels. The results from these cases were also used in a Richardson extrapolation [31] to obtain an improved estimate for the grid-resolved solution. Figure 9 shows that the loudness calculated at the ground is insensitive to the panel density in the area of the deformation, so the fine mesh was chosen to most nearly approximate the Richardson extrapolation.

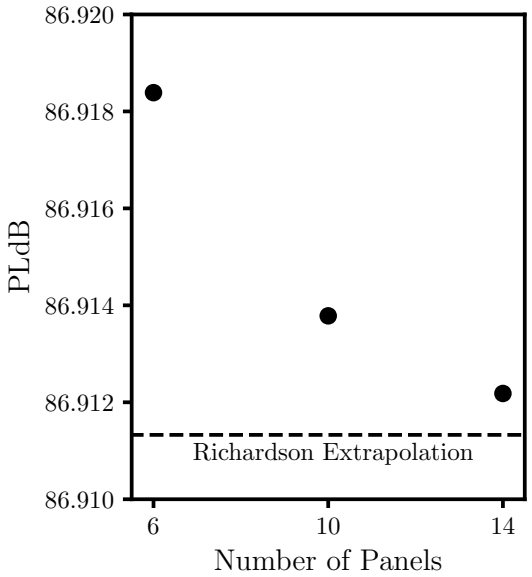

Fig. 9 Grid convergence for the deformation on the JWB-bump geometry

IV. Near-field Signature Splicing Procedure

The near-field signature splicing method outlined here is most effective when used with deformations that cause reasonably small changes in perturbation velocity. If a deformation is added to the geometry that causes a severe violation of the assumptions in PANAIR, the resulting near-field signature generated by PANAIR may have significant differences in frequency content when compared with the UNS3D near-field signature. These differences will have a direct impact on the loudness calculated from the spliced signature. It is also assumed that deformations to the geometry on this section of the aircraft are small enough that they do not significantly alter the near-field signature downstream of the deformation.

Under these conditions, the near-field signature produced by a low-fidelity solver can be spliced together with the near-field signature produced by a higher-fidelity solver and the resulting signature can be expected to produce loudness values comparable to the higher-fidelity solution. This means that the portion of the low-fidelity signature that produces accurate results can be altered through geometric morphing and produce a change in loudness at the ground that is consistent with the higher-fidelity results for the same deformation. In this work, the low-fidelity solver used is PANAIR and the higher-fidelity solver is an Euler solution from UNS3D; however, this procedure can be applied to any combination of tools that can produce a near-field signature.

After generating both low-and higher-fidelity near-field signatures for the baseline geometry, a non-dimensional axial location, x_c must be chosen where the signatures will be cut. Forward of this location, the low-fidelity signature will be used and aft of this location the higher-fidelity signature will be used. It is over the low-fidelity region forward of x_c that the design space can be explored, as anything downstream from this point will represent the baseline higher-fidelity solution. The selection of x_c at this point in the development of the method is a matter of choosing a location on the signature that captures as much of the low-fidelity signature as possible without including sections with severe violations to the assumptions of the low-fidelity model.

As there is likely a discontinuity between the signatures at x_c, a range of points on the low-fidelity signature are blended into the higher-fidelity signature. The blending function is chosen so that there is as little change to the low-fidelity signature and its frequency content as possible. If the critical point is, for example, located on the shift from a compression to an expansion, a simple linear blending function such as

$$P(x) = P(x)(1 - \omega(x)) + U_0\omega(x) \tag{2}$$

can be used, where U_0 is the first point in the higher-fidelity section of the near-field signature and ω is defined as

$$\omega(x) = \frac{x - x_b}{x_c - x_b} \tag{3}$$

where x_b is the non-dimensional axial location where blending begins. Additional blending functions could be used depending on the signature being analyzed. The combination of the blended low-fidelity signature with the higher-fidelity signature produces a spliced signature that can be propagated to the ground and analyzed to find the sonic boom loudness.

After a spliced near-field signature has been created for the baseline geometry, a near-field pressure signature generated from a deformation to the aircraft geometry forward of x_c can then be generated using the low-fidelity tools. This signature can be spliced to the baseline higher-fidelity signature using process outlined above to allow for rapid exploration of the aircraft design space. The exploration of the design space created by geometric deformations to the aircraft geometry at a constant flight condition requires only the near-field signatures from the low-fidelity tool and one higher-fidelity case with the outlined splicing method.

V. An Example of Splicing Near-field Signatures

This section will focus on a detailed description of the near-field signature splicing process on the JWB baseline geometry. Figure 10 shows the near-field pressure signature, taken at $R/L = 3$, for the JWB baseline as calculated by UNS3D and PANAIR. Significant violations of the fundamental assumptions of PANAIR begin to appear at about 80% of the reference length of the body as evidenced by the large pressure spikes. Upon examination of the near-field signatures, a value of $x_c = (x - x_0)/L = 0.87$ was selected, because it represented a point forward of which the PANAIR solution could be assumed to be reasonably accurate.

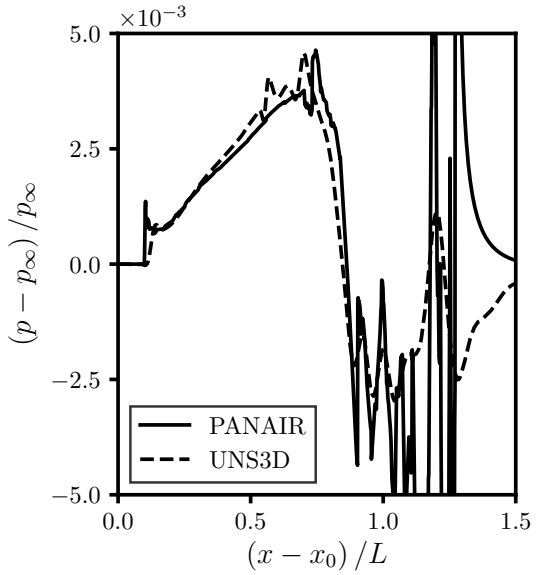

Fig. 10 Near-field pressure signatures predicted by PANAIR and UNS3D.

The partial near-field signatures left after being cut at x_c can be seen in Fig. 11. Due to the linear nature of both signatures near the cut, the large discontinuity present at x_c can be eliminated by blending the PANAIR signature using the linear blending function in Eq. (2) from $x_b = (x - x_0)/L = 0.835$ to $x_c = 0.87$. The blending range is shown in Fig. 11 for reference. The deviation of the spliced signature relative to the original signature introduced by this blending function is shown in Fig. 12. Note that the deviation shown is defined as

$$\epsilon_b = 100 * \frac{|p_{o_{\text{spliced}}} - p_{o_{\text{original}}}|}{\max\left(p_{o_{\text{original}}}\right)}\% \tag{4}$$

where p_o is the overpressure, defined by $(p - p_\infty/p_\infty)$. Figure 12 shows that the deviation of the spliced signature relative to the original signature introduced by blending was no more than 6%.

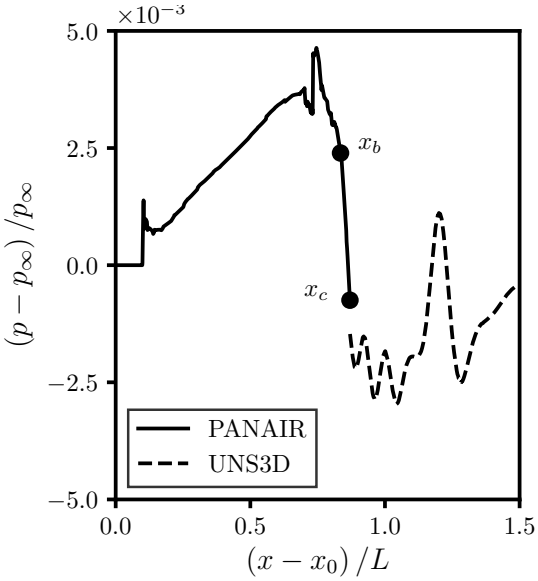

Fig. 11 Partial near-field signatures after being cut at x_c. Includes blending range from x_b to x_c.

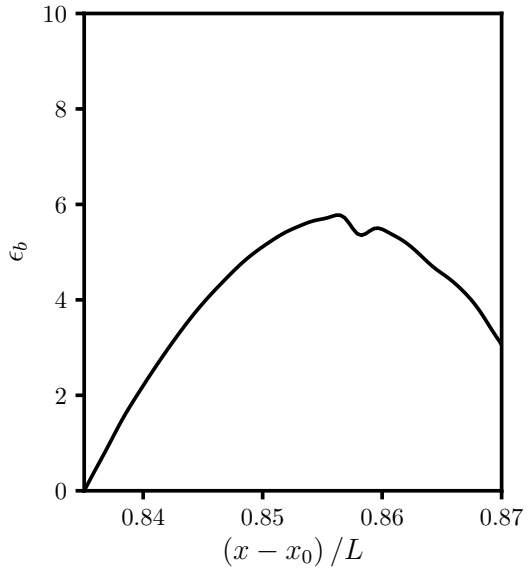

Fig. 12 Pressure deviation introduced into the PANAIR near-field signature by linear blending.

As the perceived level metric is calculated by analyzing the frequency content of a given ground signature, the deviation of the PANAIR pressure signature by the splicing process can be further examined by investigating the effect of blending on the frequency content of the ground signature. By propagating the signatures in Fig. 10 to the ground from the flight condition given in Park and Nemec [24], the power spectra can be determined for each signature.

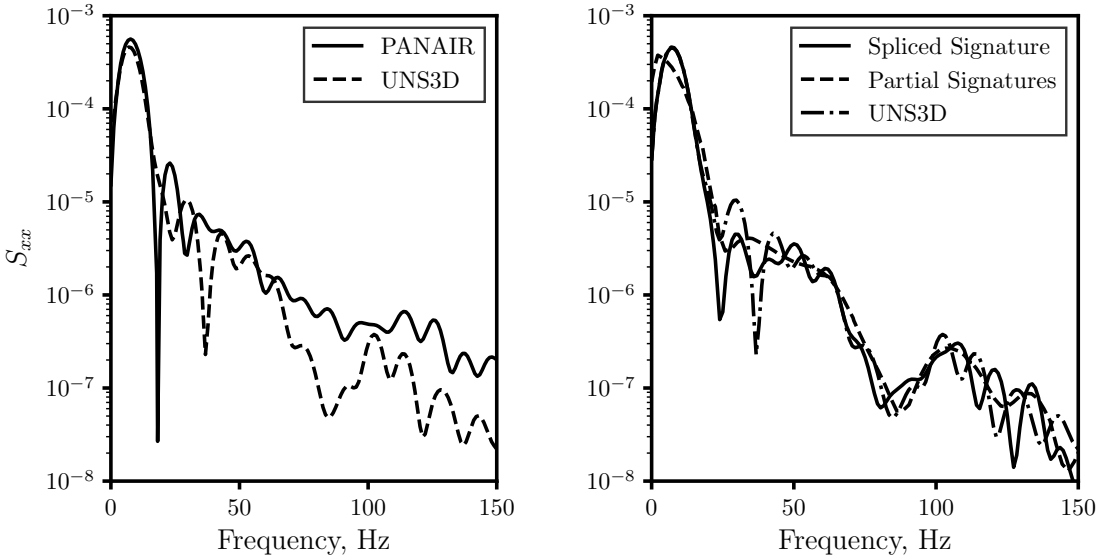

(a) Power spectra of the JWB ground signatures from PANAIR and UNS3D.

(b) Power spectra of the spliced ground signature, partial ground signatures, and the UNS3D ground signature.

Fig. 13 Power spectra plots for the baseline JWB geometry.

Figure 13a shows the differences in energy content between the PANAIR signature and the UNS3D signature over the low frequency range. Similar trends are seen in the high frequency ranges of the power spectrum as well. This indicates that the pressure spikes in the rear portion of the signature contain a significant amount of energy over a

broad range of frequencies. To quantify the difference in energy, the total power of the PANAIR signature, found by integrating the power spectrum over all frequencies, can be calculated. The total power in the PANAIR signature is 21% greater than the total power of the UNS3D power spectrum, which explains why there is such a significant difference between the loudness values of these two signatures.

As mentioned previously, a blending function should be selected that does not significantly change the power spectrum of the low-fidelity signature. This indicates that the spliced signature should have frequency content that is similar to the frequency content of the partial near-field pressure signatures shown in Fig. 11 before they are spliced. Figure 13b shows the power spectrum for the spliced signature compared to the summation of the power spectra of the partial signatures. The difference in total power between the spliced signature and the partial signatures across all frequencies is small, with a total power difference of only 4%. The total power difference in conjunction with the pressure deviation measured in Fig. 12 shows that changes in the low-fidelity signature due to splicing are small and will have little effect on the loudness of the spliced signature.

It is also helpful to compare the spliced signature to the UNS3D signature to obtain an estimate for the error in the PANAIR solution. Figure 13b shows the power spectra of the spliced signature and the UNS3D signature. The total power difference between the spliced signature and the UNS3D signature is found to be -2.5% relative to UNS3D. To identify how much of the power difference comes from splicing the signatures and how much is inherent in the differences between the PANAIR signature and UNS3D signature, the power difference can be calculated between the UNS3D and PANAIR signatures for all $(x - x_0)/L < x_c$. The difference in power between the PANAIR signature and the UNS3D signature over this range is -2.7% relative to UNS3D, therefore, splicing the signatures has created a total change in power of 0.2%, which will have little effect on the final loudness calculation. This indicates that, for this example, the splicing method used is effective at maintaining the frequency content of the original signatures.

The spliced near-field signature for the baseline geometry can be seen compared to the UNS3D signature in Fig. 14 along with the corresponding ground signatures. The near-field pressure signatures show the lack of non-linear aging present in a linearized code such as PANAIR, but indicate good agreement between the two signatures. The differences in the ground pressure signatures further indicate that there will likely be very little change in PLdB calculated between the two signatures. This is verified in Fig. 15, which shows a comparison of the loudness predictions made by the Second AIAA Sonic Boom Prediction Workshop (including a single standard deviation), PANAIR, UNS3D, and the spliced signature. The loudness in PLdB for the spliced signature was found to be 79.6, which lies within the standard deviation of the workshop results and agrees well with the loudness of 79.9 PLdB calculated from the UNS3D results.

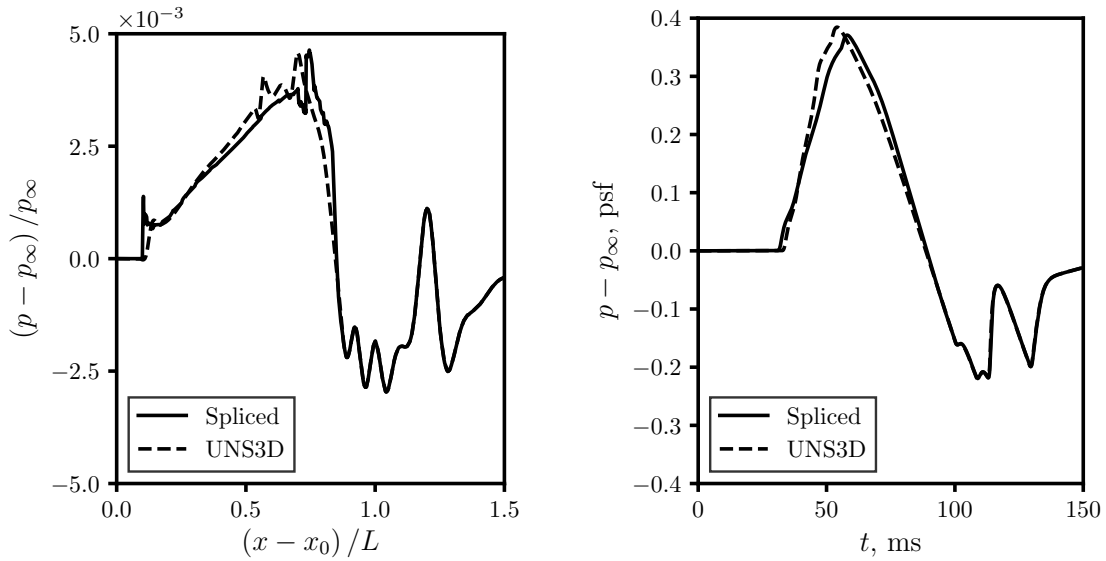

Fig. 14 Near-field and ground pressure signatures for the baseline JWB geometry.

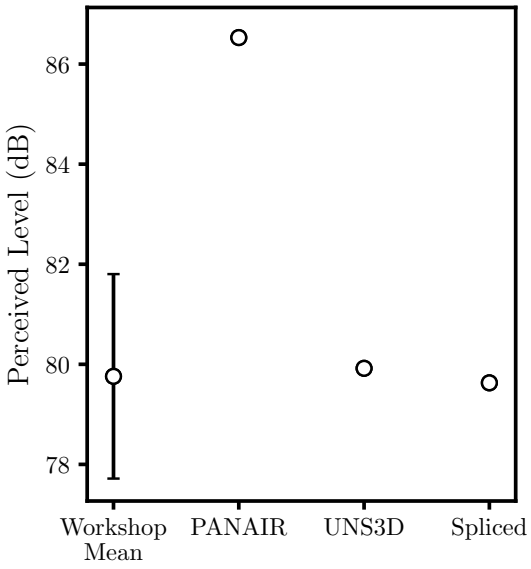

Fig. 15 A comparison of the loudness calculations for the JWB.

VI. Results for Perturbed JAXA Wing Body Geometries

Results will now be presented on the effectiveness of near-field signature splicing on the deformed JWB-bump geometry. One purpose of investigating perturbed geometries is to show that small deformations on the front of the aircraft geometry have only a small effect on the near-field signature downstream of x_c. Additionally, results from the spliced signature can be compared to the UNS3D results for the deformed geometry to determine whether the same change in loudness from the baseline is predicted.

The near-field signature generated by PANAIR for the JWB-bump geometry at $R/L = 3$ is shown alongside the signature generated by UNS3D in Fig. 16. The shock produced by the addition of the bump is clearly visible on the front of the signature. Upon further investigation, it was determined that this deformation was creating perturbation velocities that were beginning to violate the assumptions in PANAIR, as evidenced by the sharp pressure spikes at the deformation location. This large deformation was also a good test case for the limits of the splicing method in terms of deformation size.

The JWB-bump near-field signature shown in Fig. 16 was cut in the same location as the baseline geometry, $x_c = 0.87$, and the PANAIR portion of the signature was blended from $x_b = 0.835$ to x_c into the baseline UNS3D near-field signature. This blending region is indicated in Fig. 16 for reference. A near-field signature was also produced by UNS3D for the JWB-bump geometry for comparison with the spliced signature. The spliced signature for the JWB-bump geometry can be seen compared to the UNS3D solution and the corresponding ground signatures in Fig. 17. The rear part of the spliced signature, representing the UNS3D results for the baseline JWB geometry, is shown to be shifted very slightly when compared to the UNS3D solution of the JWB-bump geometry. The large pressure spikes present on the front of the PANAIR signature indicate that this deformation is beginning to seriously violate the low-perturbation velocity assumptions built into PANAIR. From this we can conclude that this deformation is near the upper limit on the deformations that can be accurately resolved using PANAIR. Since the differences between the UNS3D solutions for the baseline geometry and the deformed geometry are very small for $(x - x_0)/L > x_c$, it can be assumed that PANAIR, and not the propagation of pressure disturbances from the geometry deformation, is the limiting factor on the types of deformations used in this method. Finding precisely the limit on deformation magnitude, length, and location should be the focus of a more in-depth study in a later work.

The loudness of the spliced signature in Fig. 14 is calculated as 81.1 PLdB, which deviates from the UNS3D value of 81.5 PLdB. The difference in loudness is on the same order of magnitude as the difference between the UNS3D solution and the spliced signature for the baseline JWB geometry, but has increased slightly. This increase could be caused by the shift in the near-field signature and/or by the frequency content introduced by the pressure spikes at the location of the deformation. Regardless of their origin, these changes are still small when compared to the measured PLdB differences between UNS3D and the spliced signature for the baseline JWB and the results from the workshop. In

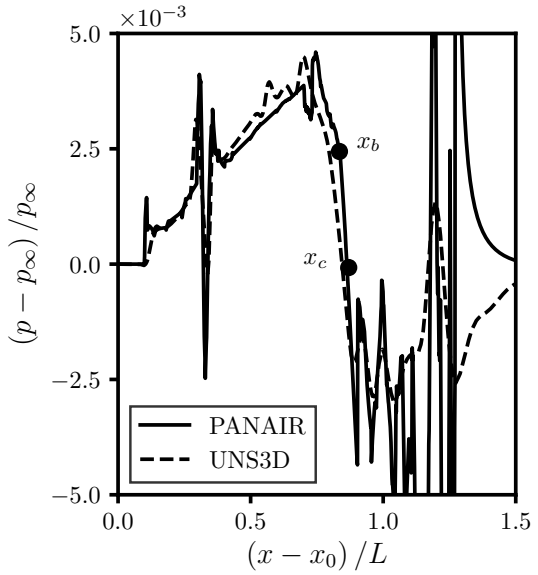

Fig. 16 Near-field signatures generated by PANAIR and UNS3D for the JWB-bump geometry. Includes blending range from x_b to x_c.

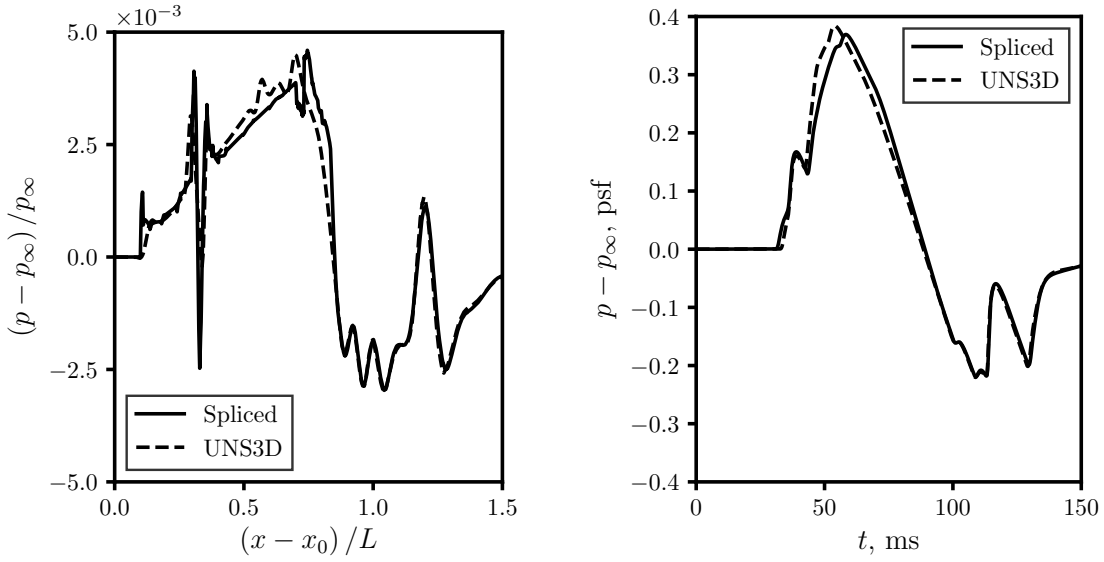

Fig. 17 Spliced near-field and ground pressure signatures for the JWB-bump geometry.

addition, the splicing technique also correctly predicts a increase in loudness with the addition of the bump. Further investigation into the power spectrum of these signatures will be necessary to determine the effects of these components on the change in PLdB.

The results discussed here indicate that, for the JWB and JWB-bump geometries, the near-field signature splicing method allows for the low-fidelity results provided by PANAIR to be spliced to a single higher-fidelity UNS3D solution and produce loudness results that are comparable to the results predicted by UNS3D. Table 2 shows a summary of the loudness values calculated for the baseline geometry and JWB-bump geometry discussed in this work. Included in this table are the loudness values in PLdB for the UNS3D solution, the PANAIR solution, and the spliced solution as well as

the change in PLdB between the various methods, where $\Delta\text{PLdB}_{\text{P-U}}$ indicates the change in PLdB between PANAIR and UNS3D, etc.

Table 2 Summary of loudness results from two deformations applied to the JWB geometry.

Geometry	UNS3D	PANAIR	Spliced	$\Delta\text{PLdB}_{\text{P-U}}$	$\Delta\text{PLdB}_{\text{S-U}}$
Baseline	79.9	86.5	79.6	6.6	-0.3
JWB-bump	81.5	86.9	81.1	5.4	-0.4
$\Delta\text{PLdB}_{\text{Baseline}}$	1.6	0.4	1.5	1.2	-0.1

A small value of $\Delta PLdB_{S-U}$ indicates that the splicing method produces loudness results that are close to the results predicted by UNS3D. The values of $\Delta PLdB_{S-U}$ measured for both the baseline JWB geometry and the JWB-bump geometry are within the limits that could be reasonably expected to appear when using a low-fidelity tool such as PANAIR. Arguably more important are the differences in loudness measured between the baseline JWB geometry and the JWB-bump geometry for UNS3D and the spliced signature. The splicing method predicts that adding the deformation in the JWB-bump geometry will increase the loudness by 1.5 PLdB, while UNS3D predicts an increase in 1.6 PLdB. The signature splicing method is effective at reducing the difference in PLdB between the UNS3D results and the initial PANAIR results and is similarly effective at matching changes in PLdB due to a geometry deformation.

The time-savings inherent in this method also deserve particular mention, since they form the basis for this method. A typical PANAIR run with the JWB geometry takes about 90 seconds on a single processor, while UNS3D takes up to 7 hours for a fine mesh on 504 Intel Xeon E5-2680 v4 2.4 GHz processors for a single configuration [5]. Since the alternative to using PANAIR would be to use higher-fidelity solvers similar to UNS3D to explore the design space, the advantages of this near-field signature splicing method are compounded by its ability to implement PANAIR for a design space study.

Future work can more clearly define the limits in deformation magnitude, length, and location for this method. Further effort will be required to identify whether the differences in PLdB between UNS3D and the spliced signatures are due to changes in the rear portion of the spliced signature or inherent in tool fidelity. These questions can be addressed by performing a small design space exploration of the JWB geometry using the splicing technique for multiple different geometry deformations at a single flight condition and examining the effects of geometry deformation on frequency content.

VII. Conclusion

A method for splicing together near-field signatures from a low-fidelity aerodynamic tool and a high-fidelity aerodynamic tool to facilitate the exploration of a design space exploration was presented and tested. This design space consists of geometric deformations on the aircraft geometry at a constant flight condition to identify locations and magnitudes of deformations to be applied to the aircraft to reduce sonic boom loudness. The near-field signature for the JAXA Wing Body geometry was produced using PANAIR, a low-fidelity tool, and found to seriously violate the basic assumptions built into PANAIR. This caused large pressure oscillations in the rear part of the geometry and in the corresponding near-field pressure signature.

As these oscillations were not found in the high-fidelity Euler solution from UNS3D, the PANAIR signature was spliced together with the near-field produced by UNS3D. A critical point was chosen at 87% of the length of the body and the signatures were blended together using a linear blending function. The frequency content of the signatures were analyzed and it was confirmed that splicing the signatures together had introduced a change of only 0.2% to the total power of the signature. In addition, the overpressure of the low-fidelity signature was changed by under 6% of the maximum overpressure, indicating that the front portion PANAIR signature had been largely unchanged by the splicing process. Evaluating the loudness of the signature using PyLdB showed that the spliced signature produced a loudness in PLdB that agreed very well with the UNS3D Euler solution and lay well within a single standard deviation of the the loudness values calculated in the Second AIAA Sonic Boom Prediction Workshop.

This method was then applied to the JWB-bump geometry, which added a Gaussian bump to the JAXA Wing Body 7.74 m from the nose with a maximum deformation of 3 cm. The PANAIR near-field signature was spliced to the UNS3D signature for the baseline JWB geometry and compared to the near-field signature computed by UNS3D for the JWB-bump geometry, which had shifted slightly with the addition of the bump. The near-field signature generated for

PANAIR by this geometry contained a large pressure spike at the location of the deformation, which indicates that the perturbation velocities along the bump were beginning to violate the assumptions built into PANAIR.

In addition, the rear portion of the UNS3D solution had shifted very slightly with the addition of the geometry deformation. From this, we conclude that, as deformations are added to the geometry, the PANAIR near-field signature solution will begin to degrade before the rear portion of the signature will change appreciably. Similar to the baseline JWB geometry, the resulting loudness showed good agreement between the spliced signature and the UNS3D signature and that the change to the frequency content was small.

Further studies should examine the specific deformation limits applicable to this method as well as isolate the changes in loudness due to frequency content and the changes due to pressure disturbance propagation from the geometry deformation. These studies should be conducted as part of an exploration of the deformation design space for the JWB geometry at a single flight condition.

By splicing together near-field pressure signatures from a low-fidelity aerodynamic solver and a high-fidelity aerodynamic solver, geometries that violate the fundamental assumptions of a low-fidelity tool can be used to explore a portion of a design space. This allows the benefits of low-fidelity solvers, more specifically the computational efficiency, to be leveraged in design space exploration while retaining an acceptable degree of accuracy. Implementation of this method will be instrumental in achieving the kind of multi-fidelity design space exploration and optimization necessary to meet the purposes of the ULI program.

Acknowledgments

This work is supported by the NASA University Leadership Initiative (ULI) program under federal award number NNX17AJ96A, titled “Adaptive Aerostructures for Revolutionary Civil Supersonic Transportation".

References

[1] Friedlander, D. J., Heath, C., and Castner, R. S., “Numerical Simulations of a Quiet SuperSonic Technology (QueSST) Aircraft Preliminary Design,” *2018 Fluid Dynamics Conference*, American Institute of Aeronautics and Astronautics, 2018. doi:10.2514/6.2018-3861, URL https://doi.org/10.2514/6.2018-3861.

[2] Ordaz, I., Wintzer, M., and Rallabhandi, S. K., “Full-Carpet Design of a Low-Boom Demonstrator Concept,” AIAA Paper 2015–2261, 2015.

[3] Ordaz, I., Geiselhart, K. A., and Fenbert, J. W., “Conceptual Design of Low-Boom Aircraft with Flight Trim Requirement,” *Journal of Aircraft*, Vol. 52, No. 3, 2015, pp. 932–939. doi:10.2514/1.C033160, URL https://doi.org/10.2514/1.C033160, 00006.

[4] Giblette, T., and Hunsaker, D. F., “Prediction of Sonic Boom Loudness Using High-Order Panel Methods for the Near-Field Solution,” *AIAA Scitech 2019 Forum*, 2019, p. 0605.

[5] Carpenter, F. L., Cizmas, P., Bolander, C. R., Giblette, T. N., and Hunsaker, D. F., “A Multi-Fidelity Optimization Study Investigating Distributed Adaptivity for Robust Low-Boom Performance,” *AIAA Aviation 2019 Forum*, 2019, p. 3237.

[6] Pierre Jr, R. L. S., Maguire, D. J., and Automotive, C. S., “The impact of A-weighting sound pressure level measurements during the evaluation of noise exposure,” *Conference NOISE-CON*, 2004, pp. 12–14.

[7] McMinn, T., “A-weighting: Is it the metric you think it is?” *Acoustics 2013*, 2013, pp. 1–4.

[8] Loubeau, A., Naka, Y., Cook, B. G., Sparrow, V. W., and Morgenstern, J. M., “A new evaluation of noise metrics for sonic booms using existing data,” *AIP Conference Proceedings*, Vol. 1685, AIP Publishing, 2015, p. 090015.

[9] Leatherwood, J. D., Sullivan, B. M., Shepherd, K. P., McCurdy, D. A., and Brown, S. A., “Summary of recent NASA studies of human response to sonic booms,” *The Journal of the Acoustical Society of America*, Vol. 111, No. 1, 2002, pp. 586–598.

[10] Stevens, S., “Perceived level of noise by Mark VII and decibels (E),” *The Journal of the Acoustical Society of America*, Vol. 51, No. 2B, 1972, pp. 575–601. 00392.

[11] Bolander, C. R., Hunsaker, D. F., Shen, H., and Carpenter, F. L., “Procedure for the Calculation of the Perceived Loudness of Sonic Booms,” *AIAA Scitech 2019 Forum*, 2019, p. 2091.

[12] Choi, S., Alonso, J. J., and Kroo, I. M., “Two-level multifidelity design optimization studies for supersonic jets,” *Journal of Aircraft*, Vol. 46, No. 3, 2009, pp. 776–790. 00075.

[13] Derbyshire, T. S., "PAN AIR summary document (version 1.0)," Tech. rep., Apr. 1982. URL https://ntrs.nasa.gov/search.jsp?R=19840020672, 00024.

[14] Ehlers, F., Epton, M., Johnson, F., Magnus, A., and Rubbert, P., "Improved Higher-Order Panel Method for Linearized Supersonic Flow," *AIAA Journal*, Vol. 17, No. 3, 1979, pp. 225–226. 00014.

[15] Medan, R. T., Magnus, A. E., Sidwell, K. W., and Epton, M. A., "PAN AIR - A Computer Program for Predicting Subsonic or Supersonic Linear Potential Flows About Arbitrary Configurations Using A Higher Order Panel Method: Volume III - Case Manual (Version 1.0)," NASA Contractor Report 3253, NASA, Ames Research Center, Aug. 1981. 00000.

[16] Baruah, P. K. B., "PAN AIR: A computer program for predicting subsonic or supersonic linear potential flows about arbitrary configurations using a higher order panel method. Volume 4: Maintenance document (version 1.1)," Tech. rep., Nov. 1981. URL https://ntrs.nasa.gov/search.jsp?R=19840025317, 00023.

[17] Epton, M. A., and Magnus, A. E., "PAN AIR: A computer program for predicting subsonic or supersonic linear potential flows about arbitrary configurations using a higher order panel method. Volume 1: Theory document (version 1.1)," Tech. Rep. NASA-CR-3251, Nov. 1981. URL https://ntrs.nasa.gov/search.jsp?R=19840019629, 00099.

[18] Sidwell, K. W., Baruah, P. K., and Bussoletti, J. E., "PAN AIR - A Computer Program for Predicting Subsonic or Supersonic Linear Potential Flows About Arbitrary Configurations Using a Higher Order Panel Method. Volume II. User's Manual (Version 1.0)." Tech. Rep. D180-24910-2, BOEING MILITARY AIRPLANE CO SEATTLE WA, May 1980. URL https://apps.dtic.mil/docs/citations/ADA093100, 00021.

[19] Ehlers, F., Johnson, F., and Rubbert, P., "A higher order panel method for linearized supersonic flow," *9th Fluid and PlasmaDynamics Conference*, American Institute of Aeronautics and Astronautics, San Diego,CA,U.S.A., 1976. doi:10.2514/6.1976-381, URL http://arc.aiaa.org/doi/10.2514/6.1976-381, 00042.

[20] Giblette, T. N., "Rapid Prediction of Low-Boom and Aerodynamic Performance of Supersonic Transport Aircraft Using Panel Methods," 2019.

[21] Chan, M. K., "Supersonic aircraft optimization for minimizing drag and sonic boom," PhD Dissertation, Stanford, California, 2003. 00025.

[22] Rallabhandi, S., and Mavris, D., "Design and analysis of supersonic business jet concepts," *6th AIAA Aviation Technology, Integration and Operations Conference (ATIO)*, 2006, p. 7702. 00002.

[23] Leal, P. B., Giblette, T., Hunsaker, D. F., and Hartl, D. J., "Extended 3D Class/Shape Transformation equations for multicomponent aircraft assemblies," *AIAA Scitech 2019 Forum*, 2019, p. 0604.

[24] Park, M. A., and Nemec, M., "Near Field Summary and Statistical Analysis of the Second AIAA Sonic Boom Prediction Workshop," *35th AIAA Applied Aerodynamics Conference*, American Institute of Aeronautics and Astronautics, 2017. doi:10.2514/6.2017-3256, URL https://doi.org/10.2514/6.2017-3256.

[25] Han, Z.-X., and Cizmas, P. G., "A CFD Method for Axial Thrust Load Prediction of Centrifugal Compressors," *International Journal of Turbo & Jet-Engines*, Vol. 20, No. 1, 2003, pp. 1–16. doi:10.1515/tjj.2003.20.1.1, URL http://dx.doi.org/10.1515/tjj.2003.20.1.1.

[26] Rallabhandi, S. K., "Advanced Sonic Boom Prediction Using the Augmented Burgers Equation," *Journal of Aircraft*, Vol. 48, No. 4, 2011, pp. 1245–1253. doi:10.2514/1.c031248, URL https://doi.org/10.2514/1.c031248.

[27] Pilon, A. R., "Spectrally accurate prediction of sonic boom signals," *AIAA journal*, Vol. 45, No. 9, 2007, pp. 2149–2156.

[28] Robinson, L. D., "Sonic Boom Propagation Through AN Inhomogeneous, Windy Atmosphere." 1991.

[29] Cleveland, R. O., "Propagation of sonic booms through a real, stratified atmosphere," Ph.D. thesis, The University of Texas at Austin, 1995.

[30] Ueno, A., Kanamori, M., and Makino, Y., "Multi-fidelity Low-boom Design Based on Near-field Pressure Signature," *54th AIAA Aerospace Sciences Meeting*, 2016, p. 2033. 00007.

[31] Richardson, L., "The approximate arithmetical solution by finite differences with an application to stresses in masonry dams," *Philosophical Transactions of the Royal Society of America*, Vol. 210, 1911, pp. 307–357.